Experimental Neurology 317 (2019) 22–33

Contents lists available at ScienceDirect

Experimental Neurology

journal homepage: www.elsevier.com/locate/yexnr

Research paper

Temporal and age-dependent effects of haptoglobin deletion on intracerebral hemorrhage-induced brain damage and neurobehavioral outcomes

Jenna L. Leclerc[a,b], Chris Li[a], Stacy Jean[a], Andrew S. Lampert[a], Claudia Loyola Amador[a], Matthew A. Diller[a], Emanuela Tolosano[c], Sylvain Doré[a,b,d,*]

[a] Department of Anesthesiology, University of Florida, Gainesville, FL, United States of America
[b] Department of Neuroscience, Center for Translational Research in Neurodegenerative Disease, McKnight Brain Institute, University of Florida, Gainesville, FL, United States of America
[c] Department of Molecular Biotechnology and Health Sciences, University of Torino, Torino, Italy
[d] Departments of Neurology, Psychiatry, and Pharmaceutics, University of Florida, Gainesville, FL, United States of America

ARTICLE INFO

Keywords:
Gliosis
Heme oxygenase
Iron
Oxidative stress
Stroke

ABSTRACT

Intracerebral hemorrhage (ICH) is a devastating stroke subtype and the presence of extracorpuscular hemoglobin (Hb) exacerbates brain damage. Haptoglobin (Hp) binds Hb, which prevents its oxidation and participation in neurotoxic reactions. Multiple studies have investigated the role of Hp under conditions of intravascular hemolysis, but little is known about its role in the brain and following ICH where extravascular hemolysis is rampant. Young and aged wildtype and $Hp^{-/-}$ mice underwent the autologous blood or collagenase ICH model. Early after ICH, $Hp^{-/-}$ mice display 58.0 ± 5.6% and 36.7 ± 6.9% less brain damage in the autologous blood and collagenase ICH models, respectively. In line with these findings, $Hp^{-/-}$ mice display less neurological deficits on several neurobehavioral tests. $Hp^{-/-}$ mice have less Perl's iron content, HO1 expression, and blood brain barrier dysfunction, but no difference in brain Hb content, astrogliosis and angiogenesis/neovascularization. At the later endpoint, the young cohort displays 27.8 ± 9.3% less brain damage, while no difference is seen with the aged cohort. For both cohorts, no differences are seen in HO1 levels or iron accumulation, but young $Hp^{-/-}$ mice display less thalamic astrogliosis and striatal microgliosis. This study reveals that the presence or absence of Hp exerts important time- and age-dependent influences on ICH outcomes.

1. Introduction

Intracerebral hemorrhage (ICH) is a form of stroke that is characterized by the accumulation of blood within the brain parenchyma. ICH is responsible for approximately 15% of all stroke cases (Sahni and Weinberger, 2007). Of these cases, 35–52% of patients die within 30 days and only 20% of those affected are able to regain functional independence, making ICH one of the most disabling forms of stroke (Caceres and Goldstein, 2012). Therapeutic medical interventions are ineffective and surgical management has not demonstrated significant improvements in mortality and functional outcomes (Kim and Bae, 2017). Studies focusing on the mechanisms of brain damage and potential treatments for ICH are crucial to decrease brain injury and improve outcomes.

ICH is a devastating neurologic event that inflicts both immediate primary injury as well as latent secondary injury. Primary damage occurs immediately following the insult and results when pressure from the hematoma mass defaces tissues and disrupts the habitual and indispensable roles of neuronal and glial cells (Keep et al., 2012). The subsequent degradation of blood initiates a cascade of events resulting in secondary injury and irreversible brain damage (Keep et al., 2012). Hemolysis causes the release of cytotoxic blood products including hemoglobin (Hb), heme and iron, which are capable of producing free radicals that go on to cause acute oxidative damage to lipids, DNA, RNA, and proteins leading to cell death (Lok et al., 2011; Wang et al., 2002). Over time, disruption of the blood brain barrier, edema and inflammation also occur and further contributes to the death of vital brain cells (Dreier et al., 2018; Liu et al., 2010; Wan et al., 2016; Zheng et al., 2016). Treatments focused on ameliorating the effects of secondary brain injury, such as preventing the toxicity associated with

* Corresponding author at: 1275 Center Drive, Gainesville, FL, United States of America.
E-mail address: sdore@ufl.edu (S. Doré).

https://doi.org/10.1016/j.expneurol.2019.01.011
Received 12 August 2018; Received in revised form 1 January 2019; Accepted 17 January 2019
Available online 19 February 2019
0014-4886/

extravascular blood products, are a putative therapeutic avenue for ICH.

Haptoglobin (Hp) is an acute phase plasma glycoprotein that binds to Hb with high affinity (K_d ~10^{-15} M) to form the haptoglobin-hemoglobin complex (Hp-Hb) (Chen-Roetling and Regan, 2016). Formation of the Hp-Hb complex stabilizes Hb, attenuates its toxic properties, and promotes the clearance of extracorpuscular Hb. The Hp-Hb complex is removed from the circulation by the reticuloendothelial system (Mehta and Reddy, 2015). Although the role of Hp in response to intravascular extracorpuscular Hb is well characterized, a paucity of literature exists investigating the role of Hp in response to hemorrhagic brain injury.

In this study, we aimed to investigate the role of Hp within the brain following ICH by using Hp knockout ($Hp^{-/-}$) mice. Contrary to our hypothesis that the presence of Hp would improve ICH outcomes, we show here the beneficial effects of genetic deletion of Hp on anatomical and functional outcomes after ICH.

2. Materials and methods

2.1. Mice

All animal procedures were approved by the University of Florida Institutional Animal Care and Use Committee, were conducted in accordance with the National Institutes of Health PHS policy on Humane Care and Use of Laboratory Animals, and reported following ARRIVE guidelines. The $Hp^{-/-}$ mice were generated from breeders provided by Dr. Emanuela Tolosano (Marro et al., 2007). C57BL/6 male mice were maintained in our temperature-controlled (23 ± 2 °C) animal facilities on a reverse light cycle (12 h light/dark) so neurobehavioral testing could be conducted during the awaken phase. This study contains two parts. In the first part, mice received either an autologous whole blood injection or collagenase-induced ICH and were sacrificed 3d post-surgery. In the autologous whole blood model, n = 10 wildtype (WT) (2.8 ± 0.1 mo) and n = 8 $Hp^{-/-}$ (3.2 ± 0.1 mo) mice were studied. In the collagenase model, n = 14 WT (4.4 ± 0.5 mo) and n = 15 $Hp^{-/-}$ (4.6 ± 0.3 mo) mice were studied. In the second part of the study, a young and aged cohort of mice underwent collagenase-induced ICH and were sacrificed 10d post-surgery. The young cohort consisted of n = 13 WT (3.3 ± 0.3 mo) and n = 12 $Hp^{-/-}$ (3.3 ± 0.1 mo) mice, and the aged cohort consisted of n = 13 WT (9.1 ± 0.3 mo) and n = 11 $Hp^{-/-}$ (9.0 ± 0.2 mo) mice. Computer-generated random numbers were used with a unique code linking to the individual animal. All surgical procedures and anatomical and functional outcomes were performed and assessed in a blinded manner. No mice were excluded from this study. Rectal temperature was maintained at 37.0 ± 0.5 °C during surgery. Mice were allowed ad libitum food and water before and after surgery and allowed to fully recover in temperature- and humidity-controlled chambers postoperatively. All possible efforts were made to reduce animal suffering. Bupivacaine was used for analgesia, hydration and wet chow was provided immediately postoperatively and daily thereafter, and animals were euthanized at humane endpoints. For euthanasia, mice were anesthetized with isoflurane and transcardially perfused with ice-cold phosphate-buffered saline followed by 4% paraformaldehyde.

2.2. Initial bleed volume

Potential differences in collagenase-induced bleed volumes in WT and $Hp^{-/-}$ mice that could confound the conclusions of this study were evaluated by measuring the brain Hb content in both groups at the peak of bleeding after collagenase-induced ICH as we have described (Leclerc et al., 2018b). A separate group of n = 4 WT and n = 5 $Hp^{-/-}$ mice were used. At 5 h after collagenase-induced ICH, mice were euthanized as described above, but without PFA perfusion. After quick removal of the brain, the olfactory bulbs, cerebellum, and contralateral hemisphere were discarded and the ipsilateral hemisphere was snap frozen. Samples were subsequently thawed, homogenized, centrifuged at 14, 000 rpm and 4 °C for 30 min, and the protein content of the supernatant was estimated using the bicinchoninic assay (ThermoFisher Scientific, Waltham, MA). Hb content was determined by enzyme-linked immunosorbent assay (Biomatik, Wilmington, DE) according to manufacturer instructions after diluting samples 1:20,000 in the kit-provided sample diluent. Results are expressed as the concentration of Hb normalized to total protein content.

2.3. Autologous blood ICH model

ICH was induced using the autologous whole blood double infusion model (30 μL total infusion) (Lok et al., 2011). Mice were anesthetized with continuous isoflurane (4% induction, 1.5–2% maintenance) and immobilized on a stereotactic frame (Stoelting, Wood Dale, IL). After making a small midline sagittal incision in the skin overlying the skull, a craniotomy was performed 0.5 mm anterior and 2.4 mm right relative to the bregma. Autologous blood was collected onto a sterile surface by needle prick of the tail artery after first cleaning the area with 70% ethanol and gently warming the tail for 2 min with a heat lamp. Blood was immediately drawn into PE-20 tubing (Instech, Plymouth Meeting, PA) connected on one side to a 50 mL syringe with a 26-gauge luer tip needle (Hamilton Company, Reno, NV) located within an automated injector, and the other side to a 26-gauge needle with the beveled end inserted into the tubing. The blunt end of this needle was inserted 3.9 mm ventral from the skull surface, removed to 3.6 mm, and left in place for 7 min. After the waiting period, 10 μL of blood was infused, followed by an additional 5 min waiting period prior to the second infusion of 20 μL. All injections were performed at 1.0 μL/min using an automated injector (Stoelting, Wood Dale, IL). The needle was left in place for 10 min after the second infusion prior to slow removal over a 25 min period.

2.4. Collagenase ICH model

ICH was induced using our described model (Leclerc et al., 2018b). Briefly, mice were anesthetized with isoflurane and immobilized in a stereotactic frame. An injection of 0.04 U collagenase type VII-S (Sigma, St. Louis, MO) dissolved in 0.4 μL of sterile water was performed at a 40° angle from the vertical plane into the left hemisphere at 0.2 μL/min using an automated injector. The injection site was 3.6 mm ventral from the skull surface at 0.0 mm anterior and 3.8 mm left relative to bregma. The needle was left in place for 5 min and then slowly removed over a 15 min period to prevent backflow.

2.5. Functional outcomes

Open field locomotor activity, rotarod, and neurological deficit scores (NDS) were used to assess functional outcomes daily post-ICH as we have described (Leclerc et al., 2015b). Behavioral tests were performed during the awaken phase (dark cycle) in the same order and at the same time of day, with 1 h rest between tests.

2.6. Measurement of serum hemopexin levels

Serum Hpx levels were measured in the 10d young and old cohorts of mice that underwent ICH as well as a separate group of naïve n = 5 WT and n = 4 $Hp^{-/-}$ mice. ELISA was used according to the manufacturer instructions (Life Diagnostics, West Chester, PA).

2.7. Histology and quantification

Histology and quantification were conducted as we have described (Leclerc et al., 2018b). Briefly, ten sets of sixteen sections equally distributed throughout the hematoma and anteroposterior brain regions

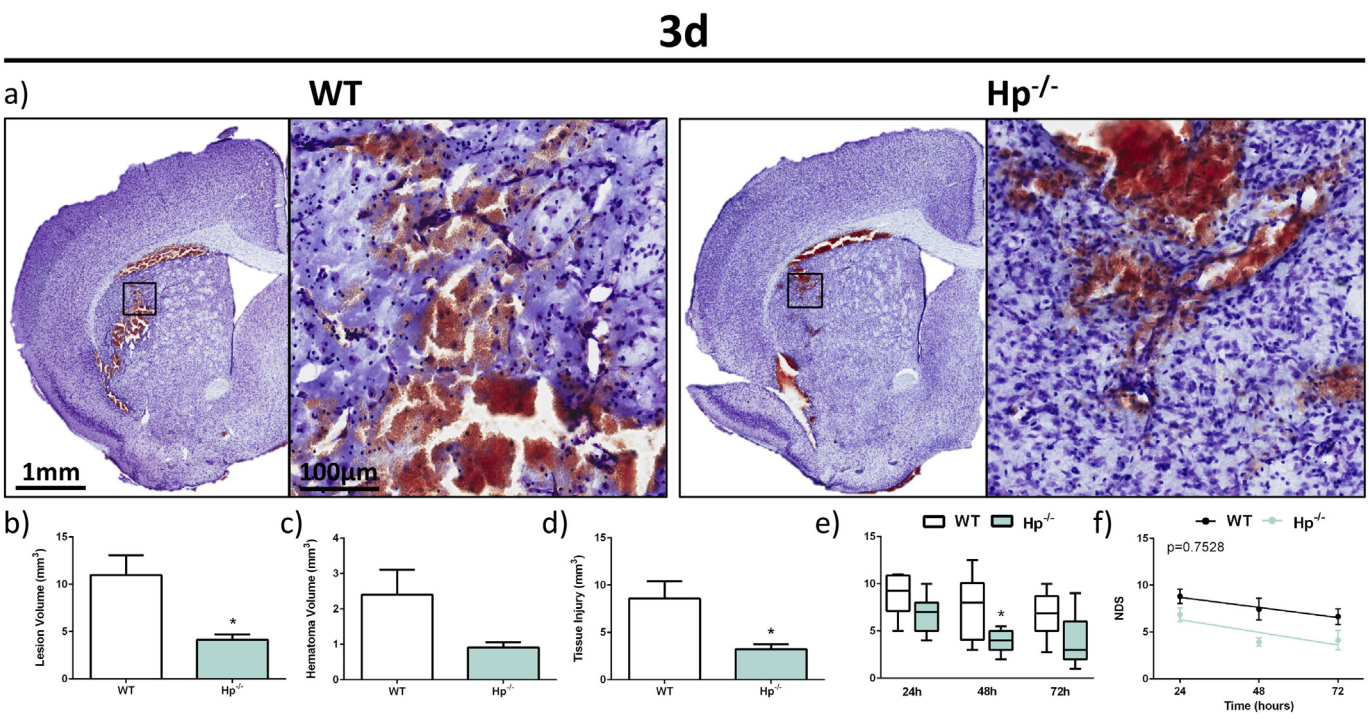

Fig. 1. Effect of Hp deletion on ICH-induced brain damage and neurobehavioral outcomes in the autologous whole blood ICH model. (a) Representative cresyl violet-stained sections are shown for WT and $Hp^{-/-}$ mice 3d following surgery at low (left) and high (right) magnification. The square on low magnification images denotes where the high magnification images were obtained from. $Hp^{-/-}$ mice have (b) smaller lesion volumes and (d) less tissue injury. (c) A trend towards smaller hematoma volumes is also seen for the $Hp^{-/-}$ mice. (e) $Hp^{-/-}$ mice have significantly less neurologic deficits on NDS at 48 h, while no differences are seen at 24 h or 72 h. (f) By comparison of the slopes on the regression analysis, no significant difference in the rate of neurological deficit recovery is seen between groups. Comparisons include n = 8 WT and n = 6 $Hp^{-/-}$ mice. *$p < .05$. (For interpretation of the references to colour in this figure legend, the reader is referred to the web version of this article.)

were processed. Cresyl violet staining was used to assess lesion and hematoma volume, tissue injury, percent ipsilateral hemispheric enlargement, and ventricular volume. Perls' iron staining was used to evaluate iron. Primary antibodies used for immunohistochemistry include heme oxygenase 1 (HO1) (1:3000; Enzo Life Sciences, Farmingdale, NY), Hb (1:500; MP Biomedicals, Santa Ana, CA), immunoglobulin G (IgG) (1:300; Vector Laboratories, Burlingame, CA), glial fibrillary acidic protein (GFAP) (1:1000; Dako, Santa Clara, CA), platelet endothelial cell adhesion molecule 1 (PECAM) (1:400; Santa Cruz, Dallas, TX), and vascular endothelial growth factor (VEGF) (1:500; Santa Cruz, Dallas, TX). For a given stain and endpoint, slides for all animals were simultaneously stained. All slides were scanned using an Aperio ScanScope CS and analyzed with ImageScope software (Leica Biosystems, Wetzlar, Germany).

For quantification of total brain pathology (lesion and hematoma volume, tissue injury, ipsilateral hemispheric enlargement, ventricular volume, HO1, iron, IgG, and Hb), all sections were quantified. For GFAP, five sections representing maximal lesion area were analyzed. For PECAM and VEGF, three sections representing maximal lesion area were used. Lesion Volume: injured brain areas were outlined. Using these areas, known distances between sections, and section thickness, a total brain lesion volume was calculated. Percent ipsilateral hemispheric enlargement: ipsilateral and contralateral hemispheres were outlined, volumes were calculated similarly to lesion volume, and the following equation was used: 100*[(ipsilateral-contralateral)/contralateral]. A positive pixel count algorithm was used for quantification of appropriately outlined brain regions for hematoma volume, iron, and immunohistochemical stains. These algorithms were tuned for each stain such that the appropriate signal level was detected (Leclerc et al., 2015b). Hematoma volume: after running the algorithm, the number of blood positive pixels were converted into an area using pixel size and a volume was calculated in an identical manner to lesion volume. Tissue injury: hematoma volume was subtracted from total lesion volume. Hb: data are presented as ipsilateral hemisphere signal normalized for contralateral hemisphere signal. GFAP: cortical astrogliosis was analyzed by placing 1000 × 1000 pixel boxes in the motor cortex. Perihematomal astrogliosis was analyzed by circling the ipsilateral and contralateral striatum, and the lesion area was excluded such that the ipsilateral analysis represents perihematomal quantification rather than a total striatal analysis. Thalamic and hippocampal astrogliosis were analyzed by circling the respective brain regions. Hemispheric astrogliosis was analyzed by circling the ipsilateral and contralateral hemispheres, excluding the lesion area. The perihematomal area was quantified to evaluate the local inflammatory response to the ICH, and the cortex and thalamus were quantified due to its connection with the striatum/perihematoma and their involvement in motor function. Hippocampal astrogliosis was evaluated due to the known cognitive impairment that occurs after an ICH (Xiong et al., 2016). Hemispheric astrogliosis was quantified to determine the global response to ICH. All GFAP measurements were calculated using positive pixel count normalized by the area of analysis. Iba1: microgliosis was determined for the cortex, striatum, thalamus, hippocampus, and hemisphere using the same procedures as for GFAP. PECAM: cortical and hematomal PECAM expression were analyzed by outlining the motor cortex and hematoma region, respectively. Ipsilateral data are reported. VEGF: was analyzed identical to PECAM, except data are presented as relative ipsilateral to contralateral signal. To specifically analyze the effect of genotype on ICH outcomes independent of the observed differences in lesion volume between the groups, each individual data point were also normalized with the corresponding lesion volume.

2.8. Statistics

Statistics were performed using SAS-JMP in consultation with a

biostatistician. Mortality was evaluated using a χ^2 test. Neurobehavioral endpoint and anatomical data were analyzed by unpaired two-tailed Student's *t*-tests. Neurobehavioral regressions were analyzed by repeated measures linear mixed modeling to account for identified baseline differences between groups and allow estimations of mortality dropouts. Additionally, the slopes were compared on these regressions to determine if differences in neurologic recovery rates were present between the genotypes. All data sets were checked for normality and differences in variance, and data was transformed or a nonparametric test was used as applicable. Data are expressed as mean ± SEM with $p < .05$ considered statistically significant.

3. Results

3.1. Effect of Hp deletion on ICH-induced brain damage

ICH-induced brain damage was determined using a variety of measurements including lesion volume, hematoma volume, tissue injury, %ipsilateral hemispheric enlargement (brain edema), and ventricular volume (hydrocephalus). At 3d after autologous whole blood ICH, $Hp^{-/-}$ mice have 58.0 ± 5.6% smaller lesion volumes (WT: 9.9 ± 2.1 mm^3, $Hp^{-/-}$: 4.1 ± 0.6 mm^3, $p = .0239$; Fig. 1b) and 57.5 ± 7.0% less perihematomal tissue injury (WT: 7.6 ± 1.9 mm^3, $Hp^{-/-}$: 3.2 ± 0.5 mm^3, $p = .0169$; Fig. 1d). The $Hp^{-/-}$ mice also tend to have smaller hematoma volumes (WT: 2.3 ± 0.6 mm^3, $Hp^{-/-}$: 0.9 ± 0.1 mm^3, $p = .0703$; Fig. 1c). At 3d after collagenase-induced ICH, $Hp^{-/-}$ mice have 36.6 ± 6.9% smaller lesion volumes (WT: 15.1 ± 1.5 mm^3, $Hp^{-/-}$: 9.6 ± 1.1 mm^3, $p = .0047$; Fig. 2b), 35.8 ± 9.5% smaller hematoma volumes (WT: 3.3 ± 0.4 mm^3, $Hp^{-/-}$: 2.1 ± 0.3 mm^3, $p = .0289$; Fig. 2c), 36.9 ± 6.6% less perihematomal tissue injury (WT: 11.8 ± 1.3 mm^3, $Hp^{-/-}$: 7.5 ± 0.8 mm^3, $p = .0036$; Fig. 2d), 50.2 ± 17.3% less edema (WT: 11.7 ± 2.2%, $Hp^{-/-}$: 5.9 ± 2.0%, $p = .0471$; Fig. 2e), and 41.8 ± 7.1% smaller ventricular volumes (WT: 5.7 ± 0.7 mm^3, $Hp^{-/-}$: 3.3 ± 0.4 mm^3, $p = .0067$; Fig. 2f).

At 10d after collagenase-induced ICH in the young cohort, $Hp^{-/-}$ mice have 27.8 ± 9.3% smaller lesion volumes (WT: 2.9 ± 0.3 mm^3, $Hp^{-/-}$: 2.1 ± 0.1 mm^3, $p = .0462$; Fig. 2h). No significant differences are seen between groups within the aged cohort ($p = .3618$; Fig. 2j).

3.2. Effect of Hp deletion on mortality after ICH

In the autologous whole blood model, two WT mice and no $Hp^{-/-}$ mice died during surgery. In the collagenase ICH 3d cohort, 2/14 WT and 0/15 $Hp^{-/-}$ mice died at the study endpoint ($p = .1292$). In the collagenase ICH 10d young cohort, 7/13 WT and 3/12 $Hp^{-/-}$ mice died at the study endpoint ($p = .1413$). In the collagenase ICH 10d aged cohort, 4/13 WT and 4/11 $Hp^{-/-}$ mice died at the study endpoint ($p = .7221$). Further inspection of the mortality data over the course of the 10d revealed that a disproportionate amount of young WT mice died within the first 4d after surgery, where 4/13 WT and 0/12 $Hp^{-/-}$ mice died during this timeframe ($p = .0360$).

3.3. Effect of Hp deletion on functional outcomes after ICH

In general, neurobehavioral outcomes following ICH are in line with the anatomical outcomes described above (Fig. 1e-f, Fig. 3). At 48 h after autologous whole blood ICH, $Hp^{-/-}$ mice have reduced neurological deficits ($p = .0205$; Fig. 1e). No significant differences are seen at 24 h ($p = .0809$; Fig. 1e) or 72 h ($p = .0622$; Fig. 1e). A slope comparison of the regression analysis showed no significant difference in the rate of recovery between groups ($p = .7528$; Fig. 1f).

For the young collagenase cohort, comparisons at the 3d endpoint show that $Hp^{-/-}$ mice have less neurological deficits on NDS ($p = .0188$; Fig. 3a), increased latency to fall ($p = .0048$; Fig. 3b), and no differences in ambulatory distance ($p = .5069$; Fig. 3c), stereotypic time ($p = .5509$; Fig. 3d), or resting time ($p = .7995$; Fig. 3e). Similarly, comparisons at the 10d endpoint reveal that young $Hp^{-/-}$ mice have less neurological deficits on NDS ($p = .0137$; Fig. 3a), increased latency to fall ($p = .0035$; Fig. 3b), and no differences in ambulatory distance ($p = .2726$; Fig. 3c), stereotypic time ($p = .4097$; Fig. 3d), or resting time ($p = .4437$; Fig. 3e). In the regression analyses, a comparison of slopes reveals no significant differences in the rate of recovery between groups for NDS, rotarod, or open field locomotor activity (Fig. 3f-j). Of note, Hp deletion improves baseline rotarod performance ($p = .0155$), decreases baseline ambulatory distance ($p < .0001$) and stereotypic time ($p = .0117$), and increases baseline resting time ($p = .0076$). Because endpoint analyses and generalized regression does not consider these baseline differences, linear mixed modeling was used to account for these differences between groups and allow estimations of mortality dropouts, such that the following comparisons reflect the effect of Hp deletion on the given outcome independent of baseline performance or the lack of data from the mice that died during the study. In these models, $Hp^{-/-}$ mice have significantly improved rotarod performance ($p = .0005$), ambulatory distance ($p = .0661$), stereotypic time ($p = .0348$), and resting time ($p = .0040$).

For the aged cohort, comparisons at the 3d endpoint for the collagenase cohort show that $Hp^{-/-}$ mice have no significant differences in neurological deficits on NDS ($p = .1466$; Fig. 3k) or rotarod ($p = .4060$; Fig. 3l), but do have reduced ambulatory distance ($p = .0355$; Fig. 3m) and stereotypic time ($p = .0167$; Fig. 3n), and increased resting time ($p = .0082$; Fig. 3o). Similarly, comparisons at the 10d endpoint reveal that aged $Hp^{-/-}$ mice have increased neurological deficits on NDS ($p = .0193$; Fig. 3k), no differences in rotarod ($p = .3809$; Fig. 3l), reduced ambulatory distance ($p < .0001$; Fig. 3m) and stereotypic time ($p = .0035$; Fig. 3n), and increased resting time ($p = .0111$; Fig. 3o). In the regression analyses for these mice, a comparison of slopes reveals no significant differences in the rate of recovery between groups for NDS, rotarod, and open field locomotor activity (Fig. 3p-t). Of note, however, Hp deletion improves baseline rotarod performance ($p = .0038$) and decreases baseline performance in all open field measurements including ambulatory distance ($p = .0124$), stereotypic time ($p = .0063$), and resting time ($p = .0175$). Using linear mixed modeling, $Hp^{-/-}$ mice have significantly decreased rotarod performance ($p < .0001$), ambulatory distance ($p = .0011$), and stereotypic time ($p = .0011$).

3.4. Effect of Hp deletion on bleed volumes after ICH

Since different initial hemorrhage volumes in WT and $Hp^{-/-}$ mice after collagenase-induce ICH could temporally influence outcomes, we assessed brain Hb content at the peak of collagenase-induced bleeding (5 h following surgery). Brain Hb content was not significantly different between WT and $Hp^{-/-}$ mice (WT: 2.4 ± 0.6 ng Hb/μg protein, $Hp^{-/-}$: 1.4 ± 0.5 ng Hb/μg protein, $p = .2488$).

3.5. Serum levels of Hpx in naïve and ICH mice

Serum levels of Hpx were measured in young and old naïve and ICH WT and $Hp^{-/-}$ mice to determine whether potential differences could confound the outcomes of this study (Table 1). Both WT (Naïve: 1.66 ± 0.15 mg/mL, ICH: 1.03 ± 0.21 mg/mL, $p = .0459$) and $Hp^{-/-}$ (Naïve: 1.89 ± 0.32 mg/mL, ICH: 1.19 ± 0.10 mg/mL, $p = .0193$) mice demonstrated significantly lower levels of serum Hpx following ICH; however, no differences were seen between genotypes for naïve young and aged mice, or in mice that underwent ICH ($p > .05$).

3.6. Effect of Hp deletion on BBB integrity after ICH

BBB dysfunction was estimated in the 3d collagenase ICH cohort using immunohistochemical staining for IgG (Fig. 4a). Compared to WT mice, $Hp^{-/-}$ mice have 48.0 ± 15.3% less IgG immunoreactivity

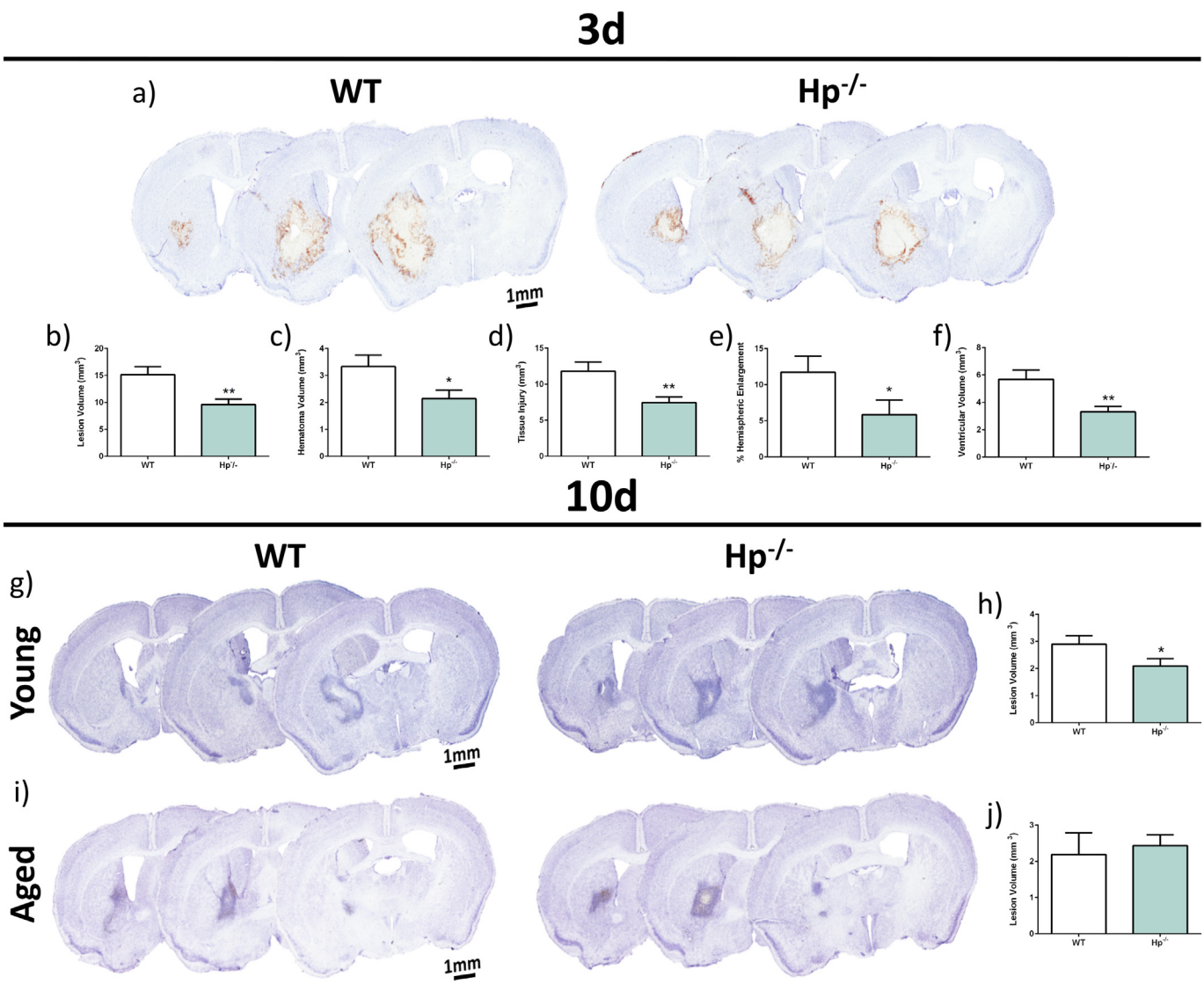

Fig. 2. Effect of Hp deletion on ICH-induced brain damage in the collagenase ICH model. Cresyl violet stained sections were used to assess a variety of outcomes to determine total brain damage. Representative sections are shown for (a) 3d, (g) young 10d, and (i) aged 10d WT and $Hp^{-/-}$ mice. Within each cohort, sections are from the same animal where left-to-right corresponds to anterior-to-posterior sections. At 3d, $Hp^{-/-}$ mice have (b) smaller lesion volumes, (c) smaller hematoma volumes, (d) less tissue injury, (e) less ipsilateral hemispheric enlargement, and (f) smaller ventricular volumes. (h) In the young 10d cohort, $Hp^{-/-}$ mice have significantly smaller lesion volumes. (j) No difference in lesion volume are seen in the aged 10d cohort. The 3d cohort includes n = 12 WT and n = 13 $Hp^{-/-}$ mice. The young 10d cohort includes n = 4 WT and n = 7 $Hp^{-/-}$ mice. The aged 10d cohort includes n = 8 WT and n = 6 $Hp^{-/-}$ mice. *$p < .05$, **$p < .01$. (For interpretation of the references to colour in this figure legend, the reader is referred to the web version of this article.)

within the ipsilateral hemisphere (WT: 4.4 ± 0.5 × 10^8 A.U., $Hp^{-/-}$: 2.3 ± 0.7 × 10^8 A.U., $p = .0412$; Fig. 4b). When individually normalized for lesion volume, this difference is no longer observed ($p = .0928$).

3.7. Effect of Hp deletion on brain Hb levels after ICH

To investigate the role of Hp in Hb clearance following ICH, immunohistochemical staining for Hb was performed in the 3d collagenase ICH cohort (Fig. 4c). Compared to WT mice, $Hp^{-/-}$ mice tend to have less Hb in the ipsilateral hemisphere 72 h following surgery, although this difference did not reach the significance threshold (WT: 4.6 ± 0.3 A.U., $Hp^{-/-}$: 3.3 ± 0.6 A.U., $p = .0772$; Fig. 4d). When individually normalized for lesion volume, still no difference is observed ($p = .5773$).

3.8. Effect of Hp deletion on HO1 and iron levels after ICH

The role of Hp in HO1 expression and iron content was determined by HO1 immunohistochemistry and Perls' iron staining (Fig. 4e-p). In the 3d collagenase ICH cohort, $Hp^{-/-}$ mice have 60.8 ± 9.6% less HO1 expression (WT: 3.4 ± 0.6 × 10^6 A.U., $Hp^{-/-}$: 1.3 ± 0.3 × 10^6 A.U., $p = .0034$; Fig. 4f) and 72.5 ± 10.8% less iron (WT: 11.5 ± 2.5 × 10^5 A.U., $Hp^{-/-}$: 3.2 ± 1.3 × 10^5 A.U., $p = .0047$; Fig. 4h) compared to WT mice. When individually normalized for lesion volume, these differences are no longer observed (HO1: $p = .1341$, iron: $p = .1286$). In the young 10d cohort, no significant differences are seen in HO1 expression ($p = .1770$; Fig. 5j) or iron ($p = .6223$; Fig. 5l). In the aged 10d cohort, no significant differences between groups are seen in HO1 expression ($p = .0614$; Fig. 4n) or iron content ($p = .6616$; Fig. 4p). When individually normalized for lesion volume, the 10d young HO1 ($p = .2271$) and 10d aged iron ($p = .4433$) remain not significant, whereas the 10d aged HO1 ($p = .0515$) and the 10d young iron ($p = .0348$) become significant.

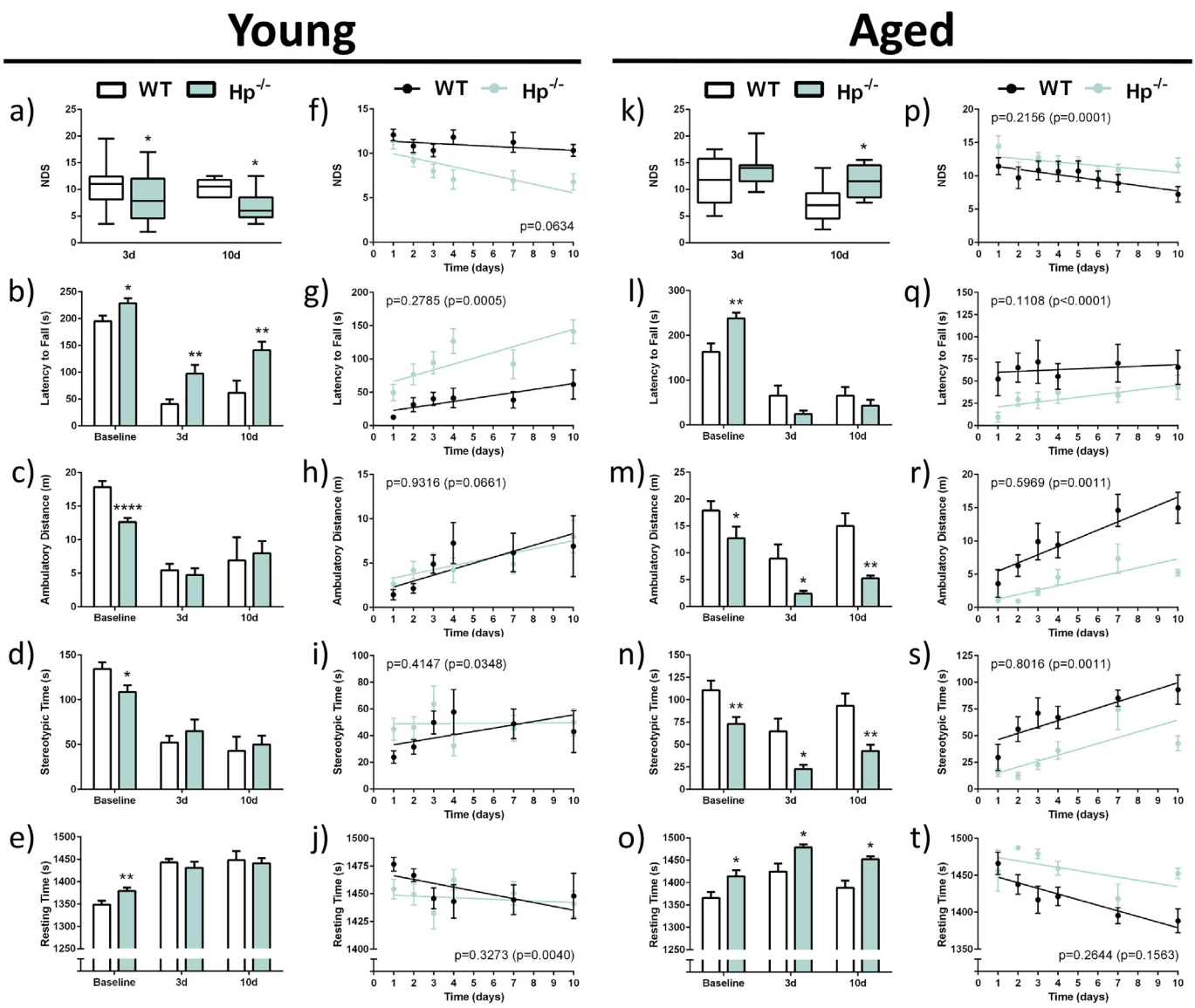

Fig. 3. Effect of Hp deletion on neurobehavioral outcomes in the collagenase ICH model. Endpoint analyses for neurological deficits on NDS, rotatrod, and open field measurements were performed at 3d and 10d for (a-e) young and (k-o) aged mice. For the young cohort, Hp deletion causes (a) decreased neurological deficit scores, (l) increased latency to fall off an accelerating rotarod, and (m-o) no differences in open field assessments at 3d and 10d post-ICH. For the aged cohort, Hp deletion causes (a) increased neurological deficit scores at 10d, (b) no differences in latency to fall off an accelerating rotarod, and (c-e) decreased performance on all open field assessments at 3d and 10d. At baseline pre-ICH induction, young and aged $Hp^{-/-}$ mice display increased latency to fall off an accelerating rotarod and decreased performance on open field measures. Two *p*-values were obtained from regression analysis in (f-j) young and (p-t) aged mice, where free-standing *p*-values represent the rate of recovery and *p*-values contained within parentheses represent differences due to genotype, independent of baseline differences and mortality dropouts (linear mixed modeling). There are no differences between genotype in rate of recovery for any neurobehavioral outcome in either the young or aged cohort. On linear mixed modeling, young $Hp^{-/-}$ mice have improved latency to fall, stereotypic time, and resting time while aged $Hp^{-/-}$ mice have decreased latency to fall, ambulatory distance, and stereotypic time. The young cohort at 3d includes n = 18 WT and n = 24 $Hp^{-/-}$ mice and at 10d includes n = 6 WT and n = 8 $Hp^{-/-}$ mice. The aged cohort comparisons include n = 9 WT and n = 7 $Hp^{-/-}$ mice. *$p < .05$, **$p < .01$, ****$p < .0001$.

Table 1
Serum levels of Hpx in young and aged WT and $Hp^{-/-}$ mice with or without ICH.

Experimental group	WT	$Hp^{-/-}$	*P* value
Naïve (young)	1.66 ± 0.15[a]	1.89 ± 0.32[b]	0.5042
10d ICH (young)	1.03 ± 0.21[a]	1.19 ± 0.10[b]	0.4668
10d ICH (old)	1.19 ± 0.22	1.28 ± 0.25	0.8051

[a] WT naïve vs. WT 10d young, $p = .0459$.
[b] $Hp^{-/-}$ naïve vs. $Hp^{-/-}$ 10d young, $p = .0193$.

3.9. Effect of Hp deletion on astrogliosis after ICH

Immunohistochemical staining for GFAP was used to evaluate astrogliosis within the ipsilateral (Fig. 5) and contralateral (Supplemental Fig. 1) cortex, striatum, thalamus, hippocampus, and hemisphere. In the 3d collagenase ICH cohort, no significant differences in astrogliosis are seen within the ipsilateral cortex ($p = .2975$; Fig. 5b), striatum ($p = .4278$; Fig. 5c), or hemisphere ($p = .2939$; Fig. 5d). No significant differences in astrogliosis are seen within the contralateral cortex ($p = .1904$; Supplemental Fig. 1b), striatum ($p = .1019$; Supplemental Fig. 1c), or hemisphere ($p = .2569$; Supplemental Fig. 1d).

In the young 10d cohort, $Hp^{-/-}$ mice have 45.8 ± 6.5% less astrogliosis within the ipsilateral thalamus (WT: 10.2 ± 0.8 A.U., $Hp^{-/}$

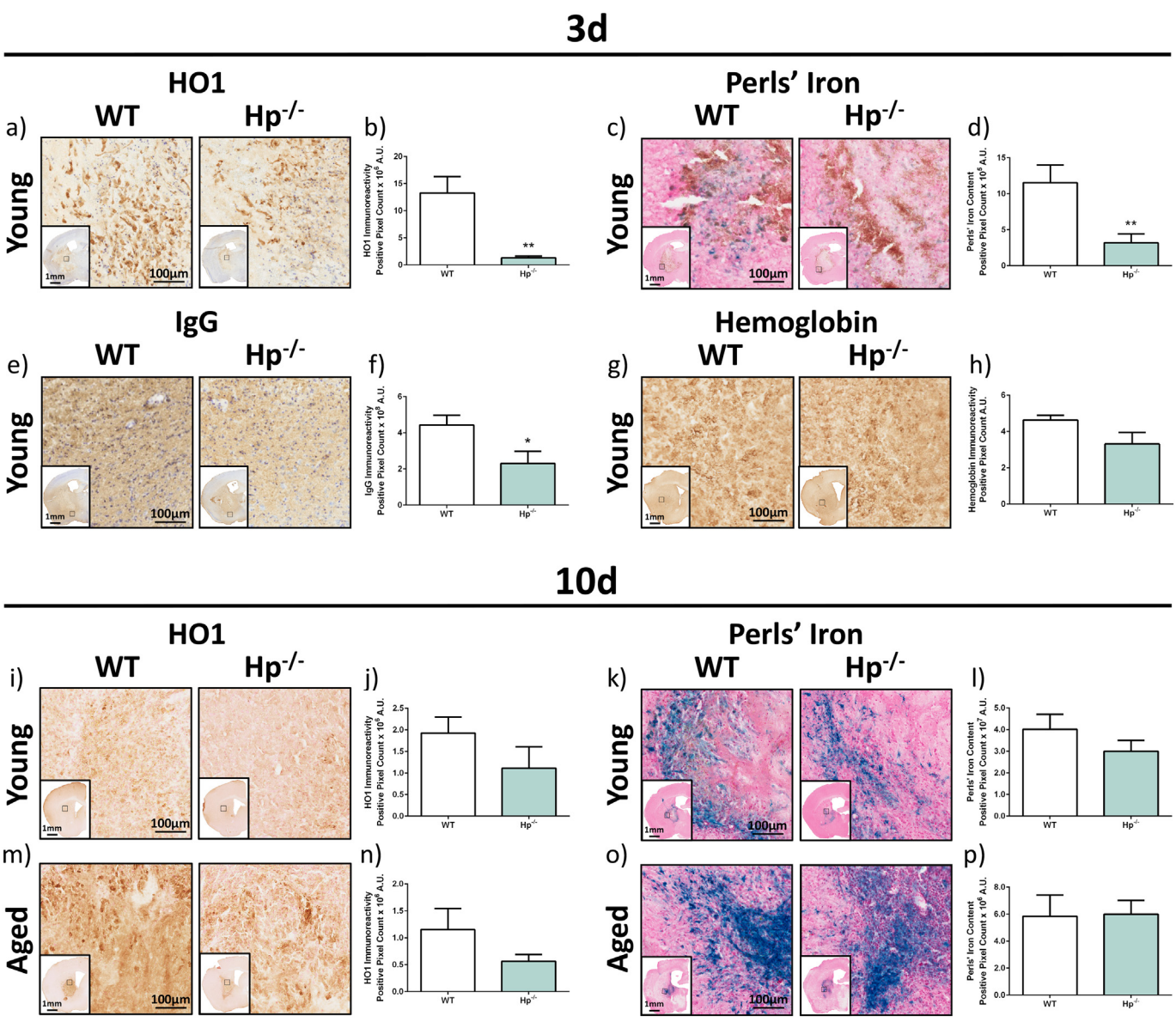

Fig. 4. Effect of Hp deletion on BBB permeability, Hb content, HO1 expression, and Perls' iron content. Immunohistochemical staining for (a) IgG and (c) Hb was used to measure BBB permeability and Hb content, respectively, for the 3d cohort that underwent the collagenase ICH model. (b) $Hp^{-/-}$ mice have less BBB permeability and (d) no difference in Hb content. Immunohistochemical staining for HO1 was used to measure HO1 expression in (e) 3d, (i) young 10d, and (m) aged 10d WT and $Hp^{-/-}$ mice that underwent the collagenase ICH model. Perls' iron staining was used to measure iron content for (g) 3d, (k) young 10d, (o) aged 10d WT and $Hp^{-/-}$ mice. At 3d, $Hp^{-/-}$ mice have (f) less HO1 expression and (h) less iron content. No differences in HO1 expression are seen for the (j) young 10d or (n) aged 10d cohorts. Similarly, no differences in iron content are seen for the (l) young 10d or (p) aged 10d cohorts. Comparisons include n = 5 WT and n = 6 $Hp^{-/-}$ mice for IgG and n = 5 WT and n = 7 $Hp^{-/-}$ mice for Hb. For HO1, comparisons include n = 9 WT and n = 12 $Hp^{-/-}$ mice for the 3d cohort, n = 3 WT and n = 5 $Hp^{-/-}$ mice for the young 10d cohort, and n = 4 WT and n = 6 $Hp^{-/-}$ mice for the aged 10d cohort. For Perls' iron, comparisons include n = 9 WT and n = 11 $Hp^{-/-}$ mice for the 3d cohort, n = 6 WT and n = 7 $Hp^{-/-}$ mice for the young 10d cohort, and n = 8 WT and n = 7 for the aged 10d cohort. *$p < .05$, **$p < .01$.

$^{-}$: 5.5 ± 0.7 A.U., $p = .0017$; Fig. 5i) compared to WT mice. Otherwise, no significant differences in astrogliosis are seen within the ipsilateral cortex ($p = .3552$; Fig. 5f), striatum ($p = .4658$; Fig. 5g), hippocampus ($p = .4349$; Fig. 5h), or hemisphere ($p = .1052$; Fig. 5j). No significant differences in astrogliosis are seen within the contralateral cortex ($p = .8596$; Supplemental Fig. 1f), striatum ($p = .6573$; Supplemental Fig. 1 g), thalamus ($p = .5528$; Supplemental Fig. 1 h), or hemisphere ($p = .7961$; Supplemental Fig. 1i).

In the aged 10d cohort, no significant differences in astrogliosis are seen within the ipsilateral cortex ($p = .2595$; Fig. 5l), striatum ($p = .6207$; Fig. 5m), hippocampus ($p = .4349$; Fig. 5n), thalamus ($p = .1241$; Fig. 5o), or hemisphere ($p = .0832$; Fig. 5p). For the contralateral hemisphere, $Hp^{-/-}$ mice have 34.1 ± 2.0% less astrogliosis (WT: 7.4 ± 0.4 × 10^{-2} A.U., $Hp^{-/-}$: 4.9 ± 0.1 × 10^{-2} A.U., $p = .0007$; Supplemental Fig. 1n). Otherwise, no significant differences in astrogliosis are seen within the contralateral cortex ($p = .0960$; Supplemental Fig. 1 k), striatum ($p = .0802$; Supplemental Fig. 1 l), or thalamus ($p = .0716$; Supplemental Fig. 1 m).

3.10. Effect of Hp deletion on microgliosis after ICH

Immunohistochemical staining for Iba1 was used to evaluate microgloisis within the ipsilateral (Fig. 6) and contralateral (Supplemental Fig. 2) cortex, striatum, thalamus, hippocampus, and hemisphere at 10d. In the young 10d cohort, $Hp^{-/-}$ mice have 55.8 ± 10.8% less ipsilateral striatal microgliosis (WT: 6.8 ± 1.7 × 10^{-2} A.U., $Hp^{-/-}$:

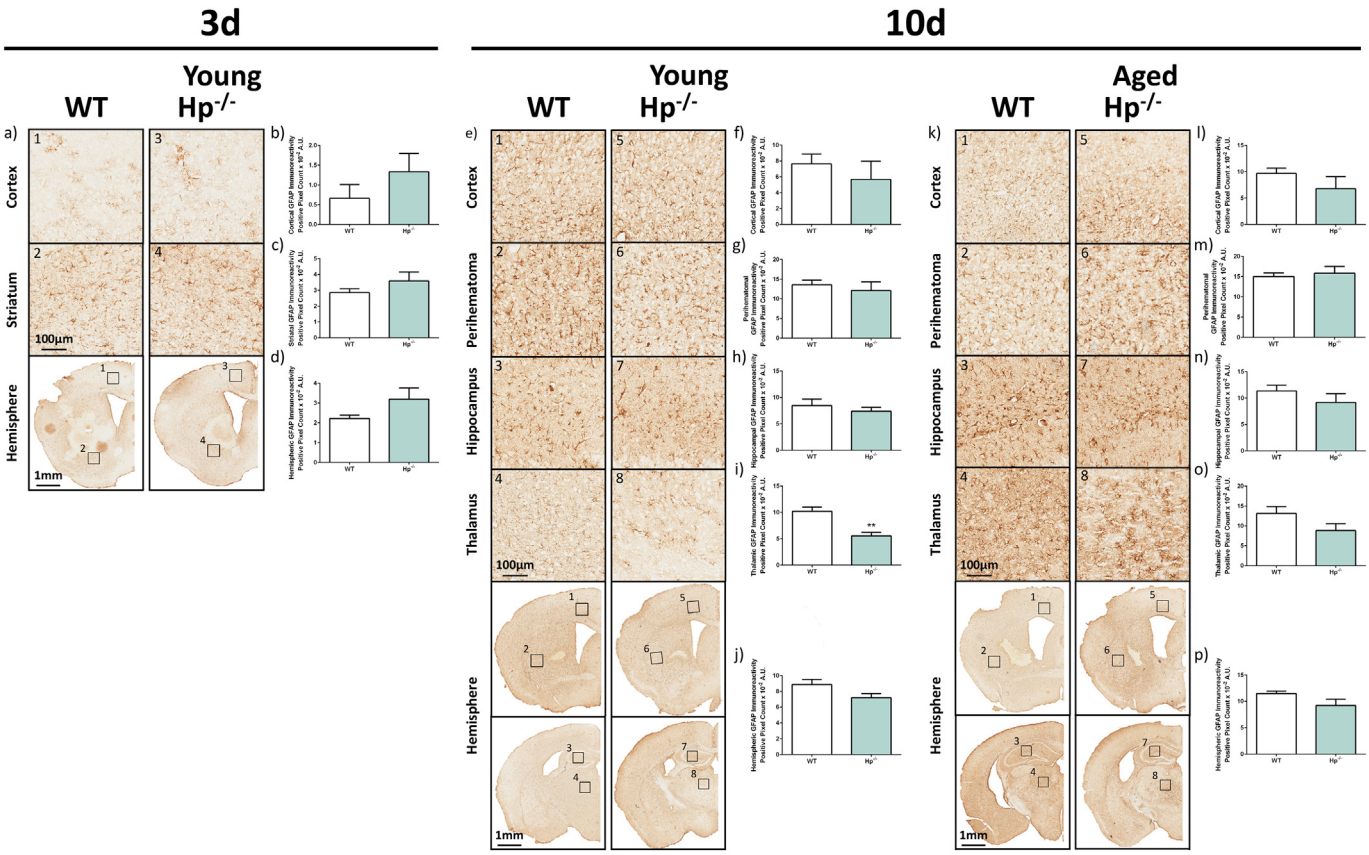

Fig. 5. Effect of Hp deletion on astrogliosis. Immunohistochemical staining for GFAP was used to evaluate astrogliosis in (a) 3d, (e) young 10d, and (k) aged 10d WT and $Hp^{-/-}$ mice that underwent the collagenase ICH model. Astrogliosis was measured in several brain regions and the numbered high magnification images correspond to the numbered boxes within the low magnification ipsilateral hemisphere images. At 3d, no differences in astrogliosis are seen within the (b) cortex, (c) striatum, or (d) hemisphere. (i) The young 10d $Hp^{-/-}$ mice have less astrogliosis within the thalamus. No differences in astrogliosis are seen within the (f) cortex, (g) striatum, (h) hippocampus, or (j) hemisphere. For the aged 10d cohort, $Hp^{-/-}$ mice have no astrogliosis differences within the (l) cortex, (m) striatum, (n) hippocampus, (o) thalamus, or (p) hemisphere. For the 3d cohort, comparisons include n = 5 WT and n = 11 $Hp^{-/-}$ mice. For the young 10d cohort, comparisons include n = 9 WT and n = 4 $Hp^{-/-}$ mice. For the aged 10d cohort, comparisons include n = 5 WT and n = 4 $Hp^{-/-}$ mice. $^{**}p < .01$.

$3.0 \pm 0.7 \times 10^{-2}$ A.U., $p = .0497$; Fig. 6c). No significant differences are seen within the ipsilateral cortex ($p = .4557$; Fig. 6b), hippocampus ($p = .5469$; Fig. 6d), thalamus ($p = .7656$; Fig. 6e), or hemisphere ($p = .4453$; Fig. 6f). No significant differences in microgliosis are seen within the contralateral cortex ($p = .9509$; Supplemental Fig. 2b), striatum ($p = .2185$; Supplemental Fig. 2c), thalamus ($p = .6101$; Supplemental Fig. 2d), or hemisphere ($p = .3250$; Supplemental Fig. 2e).

In the aged 10d cohort, $Hp^{-/-}$ mice have 43.3 ± 5.6% less ipsilateral hemispheric microgliosis (WT: $12.5 \pm 2.1 \times 10^{-3}$ A.U., $Hp^{-/-}$: $7.1 \pm 0.7 \times 10^{-3}$ A.U., $p = .0272$; Fig. 6l). No significant differences in microgliosis are seen within the ipsilateral cortex ($p = .1836$; Fig. 6h), striatum ($p = .1173$; Fig. 6i), hippocampus ($p = .0735$; Fig. 6j), or thalamus ($p = .4701$; Fig. 6k). For the contralateral hemisphere, $Hp^{-/-}$ mice have 47.4 ± 17.0% less microgliosis (WT: $6.2 \pm 0.8 \times 10^{-3}$ A.U., $Hp^{-/-}$: $3.3 \pm 1.0 \times 10^{-3}$ A.U., $p = .0304$; Supplemental Fig. 2j). No significant differences in microgliosis are seen within the contralateral cortex ($p = .1222$; Supplemental Fig. 2 g), striatum ($p = .5101$; Supplemental Fig. 2 h), or thalamus ($p = .0802$; Supplemental Fig. 2i).

3.11. Effect of Hp deletion on angiogenesis/neovascularization after ICH

Cortical and hematomal angiogenesis and neovascularization are evaluated using immunohistochemical staining for PECAM and VEGF in the 3d collagenase ICH cohort (Fig. 7). No significant differences in PECAM are seen within the cortex ($p = .3405$; Fig. 7b) or hematoma ($p = .3020$; Fig. 7c). Similarly, no significant differences in VEGF are seen within the cortex ($p = .1030$; Fig. 7e) or hematoma ($p = .2840$; Fig. 7f). When individually normalized for lesion volume, still no difference is observed for hematomal PECAM ($p = .8422$) or VEGF ($p = .7015$).

4. Discussion

In this study, we explored the role of Hp within the brain under conditions of extravascular hemolysis using two different but complementary ICH models. At 3d after the autologous model, young $Hp^{-/-}$ mice have reduced lesion volume, perihematomal tissue injury, and neurological deficit scores. At 3d after the collagenase model, young $Hp^{-/-}$ mice have less lesion and hematoma volume, perihematomal tissue injury, ipsilateral hemispheric enlargement (brain edema), and ventricular volume (hydrocephalus). These mice also show reduced neurological deficits, improved performance on an accelerating rotarod, and lower levels of HO1 expression, iron deposition, and BBB breakdown, but no differences in astrogliosis or angiogenesis/neovascularization. The possibility of Hp deletion exerting age- and time-dependent effects on ICH outcomes was explored through young and aged mice that underwent the collagenase model and were sacrificed at 10d. Young $Hp^{-/-}$ mice at 10d still show a reduction in lesion volume, while no difference is seen in the aged cohort. Similarly, young $Hp^{-/-}$ mice at 10d have less functional deficits on neurobehavioral testing, but greater deficits are seen in the aged cohort. At 10d, both the young and aged cohorts show no differences in HO1 expression or iron deposition.

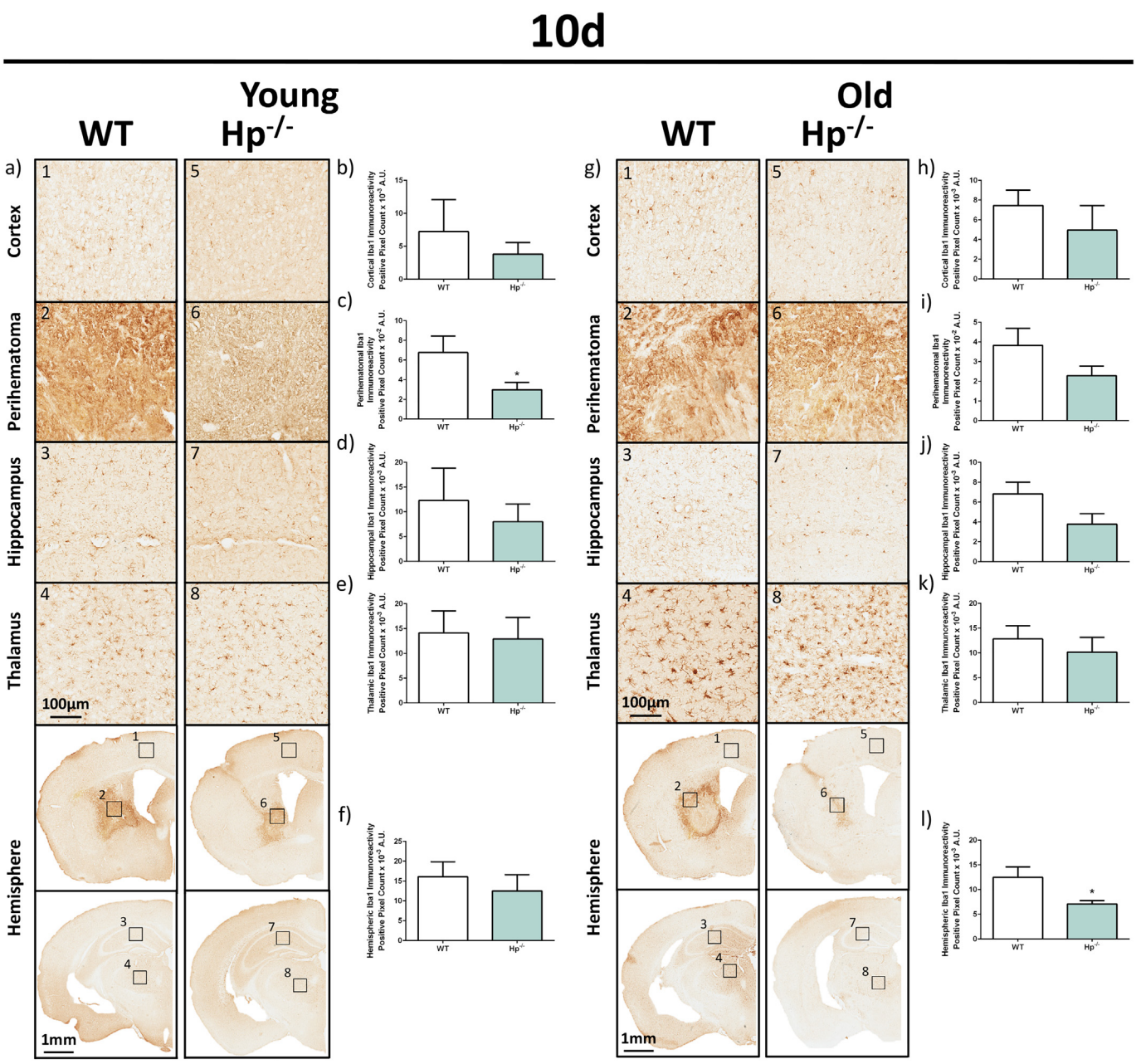

Fig. 6. Effect of Hp deletion on microgliosis. Immunohistochemical staining for Iba1 was used to evaluate microgliosis in (a) young 10d and (g) aged 10d WT and $Hp^{-/-}$ mice that underwent the collagenase ICH model. Microgliosis was measured in several brain regions and the numbered high magnification images correspond to the numbered boxes within the low magnification ipsilateral hemisphere images. (c) The young 10d $Hp^{-/-}$ mice have lower levels of microgliosis within the striatum. Otherwise, no differences are seen within the (b) cortex, (d) hippocampus, (e) thalamus, or (f) hemisphere. (l) The aged 10d $Hp^{-/-}$ mice have lower levels of microgliosis within the ipsilateral hemisphere as compared to WT controls, but no differences are seen within the (h) cortex, (i) striatum, (j) hippocampus, or (k) thalamus. For the young 10d cohort, comparisons include n = 3 WT and n = 5 $Hp^{-/-}$ mice. For the aged 10d cohort, comparisons include n = 8 WT and n = 5 $Hp^{-/-}$ mice. *$p < .05$.

The young $Hp^{-/-}$ mice do display less ipsilateral thalamic astrogliosis and perihematomal/striatal microgliosis, whereas the aged $Hp^{-/-}$ mice have less overall ipsilateral hemispheric microgliosis.

Various studies have investigated the role of Hp in the periphery under conditions of intravascular hemolysis such as hemolytic anemia, sickle cell disease (SCD), sepsis, and massive blood transfusions, where Hp functions to protect tissues from acute and/or chronic damage (Gupta et al., 2011; Quimby et al., 2015; Shih et al., 2014). Hp is one of the most abundant plasma proteins with concentrations ranging between 30 and 200 mg/dL (Chang et al., 2013; Hamalainen et al., 2012). With normal erythrocyte turnover and with mild hemolytic anemia, there is ample Hp supply to bind the free Hb released. In contrast, with more severe hemolysis, Hp levels begin to decline and can become undetectable, leaving extracorpuscular Hb, heme, and iron available to participate in toxic oxidative reactions (Schaer et al., 2014). Any formed Hp-Hb complexes are removed from the circulation via the CD163 scavenger receptor present on cells of the monocyte lineage and the toxic heme moiety is subsequently degraded by heme oxygenases (Leclerc et al., 2018b). As an example of the peripheral Hp protective effects, exogenous Hp reduces the rate of vaso-occlusion and attenuates Hb-induced HO1 expression in SCD mice, thereby reducing heme/iron mediated renal damage (Belcher et al., 2014; Chintagari et al., 2015; Shi et al., 2016). Similarly, substantial intravascular hemolysis can occur after cardiac valve repair and Hp depletion results in renal

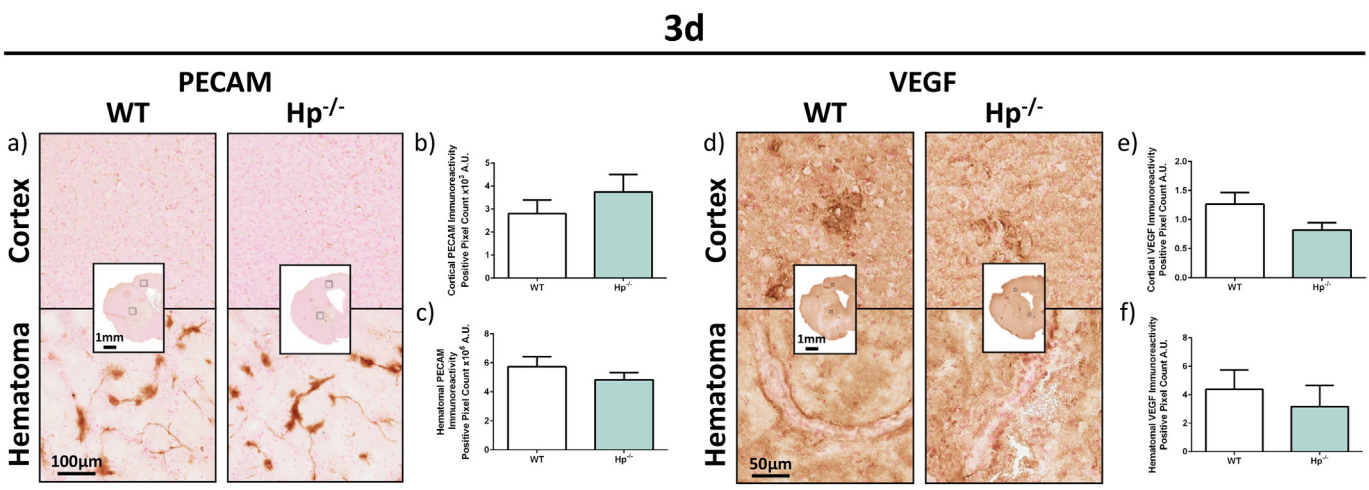

Fig. 7. Effect of Hp deletion on angiogenesis/neovascularization. Immunohistochemical staining for (a) PECAM and (d) VEGF was used to evaluate angiogenesis/neovascularization for the 3d cohort that underwent the collagenase ICH model. Angiogenesis/neovascularization was investigated within the cortex and hematoma area. No differences in PECAM expression are seen within the (b) cortex or (c) hematoma area. No differences in VEGF expression are seen within the (e) cortex or (f) hematoma area. For PECAM, comparisons include n = 5 WT and n = 9 $Hp^{-/-}$ mice. For VEGF, comparisons include n = 7 WT and n = 6 $Hp^{-/-}$ mice.

tubular deposition of hemosiderin and acute kidney injury (Qian et al., 2010).

In comparison to studies investigating the role of Hp in the periphery, significantly less literature exists regarding the role of Hp in the brain, and in particular following brain hemorrhage. Humans have two Hp alleles, resulting in three possible genotypes: Hp1–1, Hp2–1, or Hp2–2 (mice have only one Hp allele, the equivalent of Hp1–1). The Hp 2–2 genotype, which has reduced ability to detoxify Hb and is proposed to impair the clearance of Hp-Hb complexes, is associated with worse outcomes following clinical subarachnoid hemorrhage (Leclerc et al., 2015a). Similar to the present study, age-dependent effects were seen after traumatic brain injury where young and aged $Hp^{-/-}$ mice have better and worse neurologic outcomes, respectively (Glushakov et al., 2016). When compared to WT controls, $Hp^{-/-}$ and Hp-overexpressing mice had worse and better outcomes, respectively, following striatal injection of lysed erythrocytes (Zhao et al., 2009; Zhao et al., 2011). In the same study, induction of hypohaptoglobinemia via intraperitoneal injection of Hb worsened ICH outcomes and induction of Hp expression via sulforaphane improved outcomes (Zhao et al., 2009).

In contrast to the aforementioned ICH studies (Zhao et al., 2009; Zhao et al., 2011), here we show that age-matched (e.g. young) $Hp^{-/-}$ mice have improved ICH outcomes. Several possibilities exist to explain why the outcomes observed here do not align with these prior studies. Most notably, the methods used to induce the experimental ICH were different, where lysed erythrocytes were used in the former study and the collagenase and autologous whole blood models were used herein. Normally after ICH, erythrocytes are initially stable and hemolysis does not ensue until after 24 h post-bleed, and even then is initially a slow process (Wagner et al., 2003). Thus, the hemolytic timeline differences involved with the methods utilized here versus injecting pre-lysed erythrocytes may allow the brain to adapt and synthesize various molecules pre-hemolysis that could explain the differences in these studies if the response was different between WT and $Hp^{-/-}$ mice. Further complicating these hemolytic timeline differences, the study endpoints were different between the current and prior studies. Another possible explanation is the different methods used to assess ICH outcomes, both neurobehavioral testing and measures of brain damage. Of note, the differences between the prior studies and this one is not due to variability in collagenase-induced bleeding between the genotypes since no differences were seen on specific testing and our results show that young $Hp^{-/-}$ mice have less brain damage and improved functional outcomes in two separate but complementary ICH models.

Similarly, several possible explanations exist to explain the counterintuitive findings of improved outcomes with Hp gene deletion after ICH, some of which have been tested in the present study. Given that Hp is globally deleted in the $Hp^{-/-}$ mice, it is a plausible hypothesis that these mice have compensatory upregulation of other protective factors in order to handle the Hb burden, particularly those involved in Hb/heme/iron metabolism and regulatory pathways. In the absence of Hp, the toxic heme moiety is released from Hb and is predominately bound by hemopexin (Hpx), which neutralizes the deleterious oxidative effects of free extracellular heme (Wagner et al., 2003). Formation of the Hpx-heme complex leads to heme clearance by CD91/LRP1 receptor-mediated endocytosis, the degradation of heme by intracellular heme oxygenases, and the safe storage of iron by ferritin (Hvidberg et al., 2005). Here, we have shown that young and aged WT and $Hp^{-/-}$ mice with or without ICH, have no differences in serum or brain Hpx levels (Table 1, Supplemental Fig. 1). Additionally, no significant differences in HO1 or HO2 expression are seen in the brain of naïve $Hp^{-/-}$ mice compared to their WT counterparts (Supplemental Fig. 1). We also tried to test for differences in Nrf2, ferritin, ceruloplasmin, and hephaestin; however, this was unsuccessful (secondary to antibody issues, e.g. Nrf2 and ferritin are notoriously difficult to detect by the methods employed here). Along the same lines, $Hp^{-/-}$ mice could have higher levels of CD163 and under conditions of hypohaptoglobinemia it has been suggested that CD163 is able to bind and clear extracorpuscular uncomplexed Hb, thereby serving as a fail-safe Hb scavenger receptor (Etzerodt et al., 2013). Unfortunately, in the present study, we were unable to evaluate whether CD163 is locally elevated after ICH given the non-specific nature of the currently available anti-mouse CD163 antibodies as evidenced through the use of our $CD163^{-/-}$ mice (Leclerc et al., 2018b). Although, in human post-mortem brains and in a porcine ICH model, activated microglia/macrophages surrounding the clot are CD163+ and HO1+ and accumulate within the hematoma and surrounding areas over time (Cao et al., 2016; Holfelder et al., 2011). Additionally, it has been suggested that mouse Hp (in contrast to human Hp) does not promote high affinity binding of Hp-Hb complexes to CD163, but does directly bind and clear mouse Hb, and that other non-CD163 related mechanisms are contributing to Hb clearance in mice (Etzerodt et al., 2013). It should be mentioned that this prior study was conducted in the periphery rather than the brain, and thus it is possible that differences exist between systemic and CNS Hb clearance in mice and humans (Etzerodt et al., 2013). In contrast to the findings herein regarding young $Hp^{-/-}$ mice, but similar to a prior study investigating the role of Hp after traumatic brain injury, aged $Hp^{-/-}$ mice display worse neurologic outcomes

(Glushakov et al., 2016). While the reasons for these age-dependent effects are unclear, $Hp^{-/-}$ mice accumulate iron in the kidneys over their lifetime and thus the results observed here could be due to organ failure and an inability to maintain systemic homeostasis following ICH (Fagoonee et al., 2005).

Regarding the other outcomes investigated in this study, it appears that Hp gene deletion leads to reduced overall brain damage. Hb breakdown products, oxidative stress, and inflammation induce the expression of HO1 (Ferrandiz and Devesa, 2008), although interestingly 3d after ICH when these molecules are present and processes are active, we found significantly reduced HO1 expression. Given that no difference in Hb levels are seen, and $Hp^{-/-}$ mice have less HO1 and iron accumulation, these findings suggest that Hp may not be responsible for local Hb clearance/degradation after ICH. Instead, with Hp deletion, it suggests that the toxic heme moiety may possibly be cleared to the periphery. This notion is supported by our prior study demonstrating that locally expressed Hpx in the brain can clear to the periphery and be detected in plasma (Leclerc et al., 2018a). BBB dysfunction occurs after ICH and Hb breakdown products have been implicated in the pathogenesis (Keep et al., 2008). Here, we show a decrease in BBB breakdown, which further supports reduced ICH-induced brain injury with Hp gene disruption. Hp promotes angiogenesis and has been associated with regulation of arterial restructuring, especially when upregulated (Arslan et al., 2013; Cid et al., 1993; de Kleijn et al., 2002); although, no significant differences in angiogenesis/neovascularization were seen with Hp deletion after ICH, which is possibly due to the early measurement of these outcomes at 72 h post-ICH when the hematoma is starting to degrade and repair mechanisms are not in full effect. The less thalamic astrogliosis and striatial and hemispheric microgliosis is again in concordance with less neuroinflammation and overall brain damage with Hp gene deletion following ICH.

In conclusion, we demonstrate that Hp gene disruption in young mice alleviates neurologic outcomes following ICH, but aggravates outcomes in aged $Hp^{-/-}$ mice. While the exact age-dependent mechanisms for these results are unclear, these findings will open the door for further work on the Hp-CD163 scavenger pathway.

Declaration of competing interests

The author(s) declared no potential conflicts of interest with respect to the research, authorship, and/or publication of this article.

Author contributions

JLL and SD conceived and designed the study. JLL, CL, SJ, ASL, CLA, and MAD performed experiments and analyzed the data. JLL, CL, SJ, ASL, ET, and SD interpreted the results and wrote the manuscript. All authors have approved the manuscript for publication.

Funding acknowledgement

This work was supported by NIH grants F31NS086441 (JLL), R01NS046400 (SD), R21NS095166 (SD) and the McKnight Brain Research Foundation, Brain and Spinal Cord Injury Research Trust Fund (SD).

Acknowledgements

The authors wish to thank the University of Florida Center for Translational Research in Neurodegenerative Disease for support, and all members of the DorLab, and Corey Astrom, ELS.

Appendix A. Supplementary data

Supplementary data to this article can be found online at https://doi.org/10.1016/j.expneurol.2019.01.011.

References

Arslan, F., Smeets, M.B., Buttari, B., Profumo, E., Rigano, R., Akeroyd, L., Kara, E., Timmers, L., Sluijter, J.P., van Middelaar, B., den Ouden, K., Pasterkamp, G., Lim, S.K., de Kleijn, D.P., 2013. Lack of haptoglobin results in unbalanced VEGFalpha/angiopoietin-1 expression, intramural hemorrhage and impaired wound healing after myocardial infarction. J. Mol. Cell. Cardiol. 56, 116–128.

Belcher, J.D., Chen, C., Nguyen, J., Milbauer, L., Abdulla, F., Alayash, A.I., Smith, A., Nath, K.A., Hebbel, R.P., Vercellotti, G.M., 2014. Heme triggers TLR4 signaling leading to endothelial cell activation and vaso-occlusion in murine sickle cell disease. Blood 123, 377–390.

Caceres, J.A., Goldstein, J.N., 2012. Intracranial hemorrhage. Emerg. Med. Clin. North Am. 30, 771–794.

Cao, S., Zheng, M., Hua, Y., Chen, G., Keep, R.F., Xi, G., 2016. Hematoma changes during clot resolution after experimental intracerebral hemorrhage. Stroke 47, 1626–1631.

Chang, K.H., Tseng, M.Y., Ro, L.S., Lyu, R.K., Tai, Y.H., Chang, H.S., Wu, Y.R., Huang, C.C., Hsu, W.C., Kuo, H.C., Chu, C.C., Chen, C.M., 2013. Analyses of haptoglobin level in the cerebrospinal fluid and serum of patients with neuromyelitis optica and multiple sclerosis. Clin. Chim. Acta 417, 26–30.

Chen-Roetling, J., Regan, R.F., 2016. Haptoglobin increases the vulnerability of CD163-expressing neurons to hemoglobin. J. Neurochem. 139, 586–595.

Chintagari, N.R., Nguyen, J., Belcher, J.D., Vercellotti, G.M., Alayash, A.I., 2015. Haptoglobin attenuates hemoglobin-induced heme oxygenase-1 in renal proximal tubule cells and kidneys of a mouse model of sickle cell disease. Blood Cells Mol. Dis. 54, 302–306.

Cid, M.C., Grant, D.S., Hoffman, G.S., Auerbach, R., Fauci, A.S., Kleinman, H.K., 1993. Identification of haptoglobin as an angiogenic factor in sera from patients with systemic vasculitis. J. Clin. Invest. 91, 977–985.

de Kleijn, D.P., Smeets, M.B., Kemmeren, P.P., Lim, S.K., Van Middelaar, B.J., Velema, E., Schoneveld, A., Pasterkamp, G., Borst, C., 2002. Acute-phase protein haptoglobin is a cell migration factor involved in arterial restructuring. FASEB J. 16, 1123–1125.

Dreier, J.P., Lemale, C.L., Kola, V., Friedman, A., Schoknecht, K., 2018 May 15. Spreading depolarization is not an epiphenomenon but the principal mechanism of the cytotoxic edema in various gray matter structures of the brain during stroke. Neuropharmacology 134 (Pt B), 189–207. https://doi.org/10.1016/j.neuropharm.2017.09.027. Epub 2017 Sep 21.

Etzerodt, A., Kjolby, M., Nielsen, M.J., Maniecki, M., Svendsen, P., Moestrup, S.K., 2013. Plasma clearance of hemoglobin and haptoglobin in mice and effect of CD163 gene targeting disruption. Antioxid. Redox Signal. 18, 2254–2263.

Fagoonee, S., Gburek, J., Hirsch, E., Marro, S., Moestrup, S.K., Laurberg, J.M., Christensen, E.I., Silengo, L., Altruda, F., Tolosano, E., 2005. Plasma protein haptoglobin modulates renal iron loading. Am. J. Pathol. 166, 973–983.

Ferrandiz, M.L., Devesa, I., 2008. Inducers of heme oxygenase-1. Curr. Pharm. Des. 14, 473–486.

Glushakov, A.V., Arias, R.A., Tolosano, E., Dore, S., 2016. Age-dependent effects of Haptoglobin deletion in neurobehavioral and anatomical outcomes following traumatic brain injury. Front. Mol. Biosci. 3, 34.

Gupta, S., Ahern, K., Nakhl, F., Forte, F., 2011. Clinical usefulness of haptoglobin levels to evaluate hemolysis in recently transfused patients. Adv. Hematol. 2011, 389854.

Hamalainen, P., Saltevo, J., Kautiainen, H., Mantyselka, P., Vanhala, M., 2012. Erythropoietin, ferritin, haptoglobin, hemoglobin and transferrin receptor in metabolic syndrome: a case control study. Cardiovasc. Diabetol. 11, 116.

Holfelder, K., Schittenhelm, J., Trautmann, K., Haybaeck, J., Meyermann, R., Beschorner, R., 2011. De novo expression of the hemoglobin scavenger receptor CD163 by activated microglia is not associated with hemorrhages in human brain lesions. Histol. Histopathol. 26, 1007–1017.

Hvidberg, V., Maniecki, M.B., Jacobsen, C., Hojrup, P., Moller, H.J., Moestrup, S.K., 2005. Identification of the receptor scavenging hemopexin-heme complexes. Blood 106, 2572–2579.

Keep, R.F., Xiang, J., Ennis, S.R., Andjelkovic, A., Hua, Y., Xi, G., Hoff, J.T., 2008. Blood-brain barrier function in intracerebral hemorrhage. Acta Neurochir. Suppl. 105, 73–77.

Keep, R.F., Hua, Y., Xi, G., 2012. Intracerebral haemorrhage: mechanisms of injury and therapeutic targets. Lancet Neurol. 11, 720–731.

Kim, J.Y., Bae, H.J., 2017. Spontaneous intracerebral hemorrhage: management. J. Stroke 19, 28–39.

Leclerc, J.L., Blackburn, S., Neal, D., Mendez, N.V., Wharton, J.A., Waters, M.F., Dore, S., 2015a. Haptoglobin phenotype predicts the development of focal and global cerebral vasospasm and may influence outcomes after aneurysmal subarachnoid hemorrhage. Proc. Natl. Acad. Sci. U. S. A. 112, 1155–1160.

Leclerc, J.L., Lampert, A.S., Diller, M.A., Dore, S., 2015b. Genetic deletion of the prostaglandin E2 E prostanoid receptor subtype 3 improves anatomical and functional outcomes after intracerebral hemorrhage. Eur. J. Neurosci. 41, 1381–1391.

Leclerc, J.L., Santiago-Moreno, J., Dang, A., Lampert, A.S., Cruz, P.E., Rosario, A.M., Golde, T.E., Dore, S., 2018 Juna. Increased brain hemopexin levels improve outcomes after intracerebral hemorrhage. J. Cereb. Blood Flow Metab.: Off. J. Int. Soc. Cereb. Blood Flow Metab. 38 (6), 1032–1046. https://doi.org/10.1177/0271678X16679170. Epub 2016 Nov 19.

Leclerc, J.L., Lampert, A.S., Loyola Amador, C., Schlakman, B., Vasilopoulos, T., Svendsen, P., Moestrup, S.K., Dore, S., 2018 Febb. The absence of the CD163 receptor has distinct temporal influences on intracerebral hemorrhage outcomes. J. Cereb. Blood Flow Metab.: Off. J. Int. Soc. Cereb. Blood Flow Metab. 38 (2), 262–273. https://doi.org/10.1177/0271678X17701459. Epub 2017 Mar 30.

Liu, D.Z., Ander, B.P., Xu, H., Shen, Y., Kaur, P., Deng, W., Sharp, F.R., 2010. Blood-brain barrier breakdown and repair by Src after thrombin-induced injury. Ann. Neurol. 67,

526–533.
Lok, J., Leung, W., Murphy, S., Butler, W., Noviski, N., Lo, E.H., 2011. Intracranial hemorrhage: mechanisms of secondary brain injury. Acta Neurochir. Suppl. 111, 63–69.
Marro, S., Barisani, D., Chiabrando, D., Fagoonee, S., Muckenthaler, M.U., Stolte, J., Meneveri, R., Haile, D., Silengo, L., Altruda, F., Tolosano, E., 2007. Lack of haptoglobin affects iron transport across duodenum by modulating ferroportin expression. Gastroenterology 133, 1261–1271.
Mehta, N.U., Reddy, S.T., 2015. Role of hemoglobin/heme scavenger protein hemopexin in atherosclerosis and inflammatory diseases. Curr. Opin. Lipidol. 26, 384–387.
Qian, Q., Nath, K.A., Wu, Y., Daoud, T.M., Sethi, S., 2010. Hemolysis and acute kidney failure. Am. J. Kidney Dis. 56, 780–784.
Quimby, K.R., Hambleton, I.R., Landis, R.C., 2015. Intravenous infusion of haptoglobin for the prevention of adverse clinical outcome in sickle cell disease. Med. Hypotheses 85, 424–432.
Sahni, R., Weinberger, J., 2007. Management of intracerebral hemorrhage. Vasc. Health Risk Manag. 3, 701–709.
Schaer, D.J., Vinchi, F., Ingoglia, G., Tolosano, E., Buehler, P.W., 2014. Haptoglobin, hemopexin, and related defense pathways-basic science, clinical perspectives, and drug development. Front. Physiol. 5, 415.
Shi, P.A., Choi, E., Chintagari, N.R., Nguyen, J., Guo, X., Yazdanbakhsh, K., Mohandas, N., Alayash, A.I., Manci, E.A., Belcher, J.D., Vercellotti, G.M., 2016. Sustained treatment of sickle cell mice with haptoglobin increases HO-1 and H-ferritin expression and decreases iron deposition in the kidney without improvement in kidney function. Br. J. Haematol. 175, 714–723.
Shih, A.W., McFarlane, A., Verhovsek, M., 2014. Haptoglobin testing in hemolysis: measurement and interpretation. Am. J. Hematol. 89, 443–447.
Wagner, K.R., Sharp, F.R., Ardizzone, T.D., Lu, A., Clark, J.F., 2003. Heme and iron metabolism: role in cerebral hemorrhage. J. Cereb. Blood Flow Metab.: Off. J. Int. Soc. Cereb. Blood Flow Metab. 23, 629–652.
Wan, S., Cheng, Y., Jin, H., Guo, D., Hua, Y., Keep, R.F., Xi, G., 2016. Microglia activation and polarization after intracerebral hemorrhage in mice: the role of protease-activated receptor-1. Transl. Stroke Res. 7, 478–487.
Wang, X., Mori, T., Sumii, T., Lo, E.H., 2002. Hemoglobin-induced cytotoxicity in rat cerebral cortical neurons: caspase activation and oxidative stress. Stroke 33, 1882–1888.
Xiong, L., Reijmer, Y.D., Charidimou, A., Cordonnier, C., Viswanathan, A., 2016. Intracerebral hemorrhage and cognitive impairment. Biochim. Biophys. Acta 1862, 939–944.
Zhao, X., Song, S., Sun, G., Strong, R., Zhang, J., Grotta, J.C., Aronowski, J., 2009. Neuroprotective role of haptoglobin after intracerebral hemorrhage. J. Neurosci. 29, 15819–15827.
Zhao, X., Song, S., Sun, G., Zhang, J., Strong, R., Zhang, L., Grotta, J.C., Aronowski, J., 2011. Cytoprotective role of haptoglobin in brain after experimental intracerebral hemorrhage. Acta Neurochir. Suppl. 111, 107–112.
Zheng, H., Chen, C., Zhang, J., Hu, Z., 2016. Mechanism and therapy of brain edema after intracerebral hemorrhage. Cerebrovasc. Dis. 42, 155–169.